



HAL
open science

Competition between V₂O₃ phases deposited by one-step reactive sputtering process on polycrystalline conducting electrode

Jonathan Rupp, Etienne Janod, Marie-Paule Besland, Benoit Corraze, Andreas Kindsmüller, Madec Querré, Julien Tranchant, Laurent Cario, Regina Dittmann, Rainer Waser, et al.

► To cite this version:

Jonathan Rupp, Etienne Janod, Marie-Paule Besland, Benoit Corraze, Andreas Kindsmüller, et al.. Competition between V₂O₃ phases deposited by one-step reactive sputtering process on polycrystalline conducting electrode. *Thin Solid Films*, 2020, 705, pp.138063. 10.1016/j.tsf.2020.138063 . hal-02793716

HAL Id: hal-02793716

<https://hal.science/hal-02793716>

Submitted on 2 Dec 2020

HAL is a multi-disciplinary open access archive for the deposit and dissemination of scientific research documents, whether they are published or not. The documents may come from teaching and research institutions in France or abroad, or from public or private research centers.

L'archive ouverte pluridisciplinaire **HAL**, est destinée au dépôt et à la diffusion de documents scientifiques de niveau recherche, publiés ou non, émanant des établissements d'enseignement et de recherche français ou étrangers, des laboratoires publics ou privés.

1 **Title**

2 **Competition between V₂O₃ Phases Deposited by One-Step Reactive Sputtering Process on**
3 **Polycrystalline Conducting Electrode**

4

5 **Authors**

6 **J. A. J. Rupp, E. Janod, M.-P. Besland, B. Corraze, A. Kindsmüller, M. Querré, J. Tranchant,**
7 **L. Cario, R. Dittmann, R. Waser, D. J. Wouters**

8

9 **Affiliations**

10 J. A. J. Rupp, Dr. D. J. Wouters, A. Kindsmüller, Prof. Dr. R. Waser: RWTH Aachen University &
11 JARA-FIT Germany

12 Prof. Dr. R. Dittmann, Prof. Dr. R. Waser: PGI-7 Research Center Jülich & JARA-FIT Germany

13 Dr. M. Querré, Dr. M.-P. Besland, Dr. E. Janod, Dr. L. Cario, Dr. J. Tranchant : Institut des

14 Matériaux Jean Rouxel (IMN) Université de Nantes, CNRS, France

15

16 **Abstract**

17 This comprehensive work investigates a technologically appealing synthesis of V₂O₃ oxide thin
18 films for electronic applications by the use of direct reactive sputtering with a heavily diluted
19 gas mixture on a conducting platinum electrode. Morphological characterization was
20 performed by Scanning Electron Microscopy, Atomic Force Microscopy , X-Ray Diffraction and
21 X-Ray Reflectometry. Vanadium valence states were investigated by X-Ray Photoelectron
22 Spectroscopy and crystalline phases were checked by X-Ray Grazing Incidence measurements.
23 Low temperature electrical transport characteristics were determined by 2-point probe
24 measurements. Only amorphous V₂O₃ was found to exist in a mixed-valence phase in the

1 investigated parameter range. Deposition temperatures between 400 °C and 550 °C enable
2 formation of mixtures between crystallographic phases of corundum- and bixbyite-type V_2O_3
3 polymorphs. Depending on temperature and sputtering power, morphology and
4 stoichiometry can be tuned to generate four distinct type of electrical transport
5 characteristics. Most promising electrical properties of corundum V_2O_3 with a resistance ratio
6 of up to four orders of magnitude (during the low temperature insulator-to-metal transition)
7 have been obtained for a moderate sputtering power of 50 W (on a 1" target) at a deposition
8 temperature of 600 °C. Reactive sputtering thus enables direct control of structural and
9 electrical parameters for polycrystalline V_2O_3 thin film phases on a conducting substrate.

10

11 **Key Words**

12 Vanadium Oxide, Vanadium Sesquioxide, V_2O_3 , Reactive Sputtering, Bixbyite.

13

14 **1. Introduction**

15 The vanadium-oxygen system comprises a large variety of over 20 thermodynamically stable
16 crystalline phases throughout the range of oxygen content [1]. Most of these phases exhibit
17 fascinating chemical and physical features that open a large field of technical applications [2].
18 For instance, vanadium based oxides have attracted much attention in energy storage systems
19 operating with lithium and sodium batteries [3] which are regarded as the most promising
20 electrochemical storage technologies. Furthermore, the famous low oxygen content phase of
21 VO_2 was widely proposed for usage in optical [4][5] and electrical switches [6][7]. Yet,
22 controlled synthesis of phases with uniform stoichiometry (in particular phases with a low
23 oxygen to vanadium ratio of $O:V < 2.5$) is highly challenging because it requires precise control
24 of low oxygen partial pressures $p(O_2)$ besides the need for high crystallization temperatures.
25 Another well-known phase with even lower oxygen content is the correlated metal of

1 corundum V_2O_3 which undergoes an insulator-to-metal transition (**IMT**) at 155 K from a
2 paramagnetic metallic phase to a low temperature antiferromagnetic insulating monoclinic
3 phase [8]. The crystallographic phase change leads to a drop of the c/a ratio and a volume
4 increase of about 1.2 % accompanied by a change in resistivity up to six orders of magnitude.
5 More interestingly, under tensile strain, V_2O_3 is regarded being an archetype Mott-Hubbard
6 insulator [8]. On atomic scale, an equivalent negative (chemical) pressure can be ensured by
7 doping of V_2O_3 with over 1.1 at. % chromium. This kind of material can realize an IMT without
8 crystallographic phase change which can be driven not only by pressure or temperature [8]
9 but also by an electric potential [9]. While transitions of pure vanadium oxide phases are
10 volatile phenomena [10][11], non-volatile resistive switching could be realized as well in Cr-
11 doped V_2O_3 with at least 5 at. % Cr [12]. This makes the family of vanadium oxides (and
12 especially un-doped and Cr-doped V_2O_3) an interesting candidate for the fabrication of
13 electrical devices for neuromorphic [13] and memory applications [12].

14 In the past, many different synthesis methods have been involved to obtain low oxygen
15 content phases such as V_2O_3 . Typically, equilibrium synthesis relies on a two-step approach
16 with deposition and subsequent reduction, e.g. thermal reduction [14], oxygen buffer
17 reduction [15] or plasma hydrogen reduction [16]. Alternatively, direct deposition of low
18 oxygen content phases is only achieved by non-equilibrium synthesis, e.g. molecular beam
19 epitaxy [17][18], electron beam evaporation [19][20][21] or reactive sputtering [22][23]. For
20 various techniques, it has been confirmed that the oxygen partial pressure mainly determines
21 the phase to be formed [24][25][26][27]. Previous works with direct deposition methods
22 typically used substrate temperatures between 700 °C [28][29] and 1700 °C [24] to ensure
23 satisfying thin film crystalline quality. With reactive sputtering, we chose a deposition
24 technique compatible with a standard CMOS fabrication and giving access to a large range of

1 physical layer properties such as morphology, roughness and density. Strong deviations from
2 well-known bulk properties have already been identified for “ideal” epitaxial V_2O_3 thin films
3 grown on insulating sapphire due to various effects such as porosity [30] and residual stress
4 [24]. For technological purposes in electronic devices, the physical properties of V_2O_3 thin films
5 should further be investigated in polycrystalline form on a polycrystalline conducting
6 electrode. Using a conducting electrode as substrate can ensure an electrical contact for the
7 fabrication of resistively switching devices based on a capacitor structures in a desired vertical
8 metal-insulator-metal (**MIM**) geometry. Apart from the deposition of aforementioned
9 crystalline films, amorphous oxide semiconductors are a hot topic in materials science and
10 engineering as well [31] thanks to their highly promising benefits such as lowest deposition
11 temperature, high resistivity, low roughness and attainable uniform and isotropic properties.
12 Therefore, the realization of amorphous Cr-doped V_2O_3 thin films as “precursor” is a further
13 valuable goal that is of interest e.g. for selector devices [32][33].

14 Here we present a comprehensive and systematic optimization of a direct deposition method
15 for V_2O_3 in amorphous and crystalline form on a conducting electrode. For the lowest
16 deposition temperature at room temperature, V $3+$ valence only manifests in combination
17 with $+2$ or $+4$ valences for the investigated parameters. Crystalline V_2O_3 could be achieved at
18 a minimum deposition temperature of $400\text{ }^\circ\text{C}$. However, slight variations in oxygen partial
19 pressure lead to additional formation of metastable bixbyite-type V_2O_3 up to $550\text{ }^\circ\text{C}$. A
20 moderate sputtering power of 50 W and a deposition temperature of $600\text{ }^\circ\text{C}$ resulted in pure
21 corundum V_2O_3 phase with a clear insulator-to-metal transition and resistance ratio of four
22 orders of magnitude. Direct reactive sputtering can thus be considered as a valuable technique
23 to control structural and electrical features of V_2O_3 thin films on a conducting substrate such

1 as platinum. Moreover, it gives a physical synthesis method for the metastable compound of
2 bixbyite V_2O_3 .

3

4 **2. Experimental**

5 Various vanadium oxide thin films (with a thickness ranging from 30 nm to 120 nm) have been
6 deposited on a 30 nm thick platinum bottom layer by radio frequency (**RF**) reactive magnetron
7 sputtering of a one inch vanadium target. Off-axis co-sputtering with an incident angle of 15°
8 was used. The target to substrate distance was fixed at 5 cm. The base pressure was held
9 below $p_{\text{base}} < 1$ nbar and the working pressure was fixed at $p_{\text{process}} = 10$ μ bar. The oxygen
10 partial pressure $p(O_2)$ was adjusted with a flux ratio of two mass flow controllers: pure Argon
11 and an Oxygen/Argon mixture allowing various flow rate ratios: 100/0 (with access to a $p(O_2)$)
12 ranging from 1000 to 100 nbar), 10/90 (100 nbar to 10 nbar range) or 1/99 (10 nbar to 1 nbar
13 range). With such ratios, the used oxygen partial pressure was straightforwardly calculated
14 with the assumption of an ideal gas. This method allowed control of the $p(O_2)$ down to a
15 few nanobar. Several series of vanadium oxide thin films were deposited as summarized in
16 **Table 1 to 4**: three sample series were fabricated while varying oxygen partial pressure
17 between 1000 nbar and 1 nbar. The sample "series 1" was sputtered at room temperature
18 ($T = 30$ °C, $P = 100$ W, **Table 1**) and two samples "series 2" and "series 3" were sputtered at
19 elevated substrate temperatures with different sputtering powers P ($T = 400$ °C, $P = 100$ W,
20 **Table 2** and $T = 400$ °C, $P = 50$ W, **Table 3**, respectively). Two sputtering power values were
21 investigated since a strong increase in deposition rate by one order of magnitude was
22 obtained in the lower oxygen partial pressure range (see Figure 1). A fourth sample "series 4"
23 explores the temperature dependence of V_2O_3 from room temperature up to 600 °C for a
24 $p(O_2)$ of 10 nbar (**Table 4**) with a deposition power of 50 W. For the fifth series 5 (not shown)

1 deposited with a power of 100 W (i.e. increase of sputtering power by a factor of two),
2 crystalline phases were determined by XRD. For the determination of the thickness of
3 vanadium oxide films (and calculation of their deposition rate), X-ray reflectometry (**XRD:XRR**)
4 was performed with an X-ray diffractometer by PANalytical. The thickness was extracted by
5 evaluation of the Kiessing fringes of the relevant vanadium oxide layer on the substrate.
6 Densities of vanadium oxide thin films were simulated with the obtained intensity reflection
7 profile and the software X'pert reflectivity from PANalytical. Hereby, a substrate stack of SiO₂
8 (thickness $d = 600 \mu\text{m}$, density $\rho = 2.32 \text{ g/cm}^3$, mean root square roughness $R_{\text{ms}} = 0 \text{ nm}$)
9 followed by an adhesion layer TiO_x ($d = 5 \pm 1 \text{ nm}$, $\rho = 3.28 \text{ g/cm}^3$, $R_{\text{ms}} = 0-1 \text{ nm}$) and the
10 electrode Pt ($d = 30 \text{ nm}$, $\rho = 21.2 \text{ g/cm}^3$, $R_{\text{ms}} = 0-1 \text{ nm}$) served as input with given simulation
11 constraints. During the segmented fit, values for thickness, density and roughness of the
12 vanadium oxide film on top of the substrate were kept variable. For selected samples, the
13 vanadium valence was determined as function of oxygen partial pressure by X-ray
14 photoelectron spectroscopy (**XPS**) at a "PHI 5000 Versa Probe II" from Ulvac-Phi, Inc. with an
15 energy resolution better than 0.2 eV. Peaks were normalized to the C 1s binding energy of
16 residual carbon. In particular, vanadium V2p core level spectra were recorded and
17 stoichiometry was determined while comparing obtained spectra with integer vanadium
18 oxidation states. These binding energies were determined by analysing reference samples of
19 crystalline vanadium oxide thin films V₂O₅, VO₂, V₂O₃ and VO, (see Table 2&3) as well as
20 through comparison with literature values^{[34][35]}. To avoid photoelectron signal from native
21 oxidation after sputtering, vanadium oxide thin films were capped *in situ* by a 100 nm thick Au
22 layer. The capping layer was further stripped off with scotch tape and manipulator in the XPS
23 chamber high vacuum system right before the measurement. The pure vanadium thin film
24 (without capping layer) was etched by Argon ion sputtering to remove native oxidation.

1 Oxidation states of amorphous VO_x thin films were determined for some critical $p(\text{O}_2)$ values
2 (where major changes in deposition rate were observed) by XPS. Due to the complex shape of
3 V 2p core level spectra of vanadium oxide phases, fitting was not performed. Oxidation states
4 are here discussed qualitatively by their energy position with respect to integer valence states.
5 For crystalline thin films, crystallographic phases were determined using X-ray diffractometry
6 in grazing incidence geometry **XRD:GI** with a diffractometer “X’Pert PRO” from PANalytical
7 with a Cu-K_α source. The volume ratio of corundum and bixbyite V_2O_3 was determined by
8 refinement of diffraction patterns via PowderCell software. The use of grazing incidence mode
9 and a possible preferential orientation of corundum V_2O_3 results in an uncertainty of about
10 ± 5 vol. %. Thus, given estimations should be considered as qualitative guideline. To determine
11 the optical reflectance of the deposited films, Light Microscopy images were taken in a
12 controlled environment (clean room yellow lightning, constant brightness and contrast) at
13 magnification 50 by an “Olympus MX 50” microscope. Morphology was determined by
14 scanning electron microscopy (**SEM**) using a Zeiss “DSM982 GEMINI” electron microscope with
15 an operating voltage of 10 kV. Grain sizes were determined using the line section method with
16 SEM images and roughness was quantified using an atomic force microscope (**AFM**) from
17 Veeco “di CP II”. Low temperature electrical transport characteristics were performed with a
18 modified closed-cycle Helium circuit cryostat “Omniplex DE210” from ARS.

19

20 **3. Results**

21 In **Table 1**, deposition rates dd/dt as well as detected vanadium valences are given for samples
22 sputtered at room temperature (30 °C) as a function of oxygen partial pressure. Numbers in
23 brackets give secondary valence states with minor quantitative occurrence. **Table 2** and **3**
24 summarize deposition rates, detected phases as well as analysis of vanadium valences of

1 samples sputtered at 400 °C for samples sputtered at 100 W and 50 W, respectively. In the
2 following sections, the trends of physical parameters of deposited films will be presented and
3 discussed.

4

5 **3.1 Deposition Rates of Thin Films Sputtered at 30 °C / 400 °C / 600 °C**

6 In **Figure 1**, the deposition rate is plotted as function of logarithmic oxygen partial pressure
7 for samples sputtered at room temperature (blue squares) and at 400 °C (green dots)
8 (series 1&2). For samples sputtered at room temperature (blue squares), four distinct regimes
9 can be identified (labelled as zones (1) to (4)): In the case of a high oxygen partial pressure of
10 400 nbar, a very slow deposition rate of 0.5 nm/min is obtained which slightly decreases with
11 increasing $p(\text{O}_2)$ (zone (1)). Towards lower oxygen partial pressure (zone (2)), the deposition
12 rate increases by one order of magnitude up to 8.8 nm/min and reaches its maximum at a
13 $p(\text{O}_2)$ of 100 nbar. In an intermediate regime in zone (3) (for a $p(\text{O}_2)$ between 100 nbar and
14 10 nbar), the deposition rate stays constant whereas for oxygen partial pressures below
15 10 nbar (zone (4)), the deposition rate drops to a value of 5 nm/min. For thin films deposited
16 at 400 °C (green dots), one can observe a similar trend as for the ones sputtered at 30 °C for
17 the same sputtering power of 100 W. In contrast to thin films sputtered at room temperature,
18 a stronger variation of absolute deposition rate values spans up a range of ~2 nm/min. For
19 thin films sputtered with half the power on the target (50 W, Figure 1 inset), the deposition
20 rate is decreased by a factor of two (3.3 nm/min) as compared to the rate obtained at 100 W
21 (6.7 nm/min). Furthermore, a variation of deposition temperature from 400 °C to 600 °C only
22 leads to a marginal change in deposition rate at low power of 50 W (~0.5 nm/min) but a more
23 significant one at a higher power of 100 W (~1.5 nm/min).

24

3.2 Phase Analysis of Thin Films Sputtered at 30 °C / 400 °C / 600 °C

1 **Figure 2** (a)-(d) display XRD:GI patterns of thin films sputtered at 400 °C with integer vanadium
2 valence across the entire investigated oxygen partial pressure range. In most cases of
3 investigated thin films, a mixture of at least two different phases was obtained (as summarized
4 in Table 2&3). For certain conditions of oxygen partial pressure (Figure 2), pure vanadium
5 oxide phases were detected with V_2O_5 (400 nbar, (a)), VO_2 (70 nbar, (b)), V_2O_3 (6 nbar, (c)) and
6 V_2O_2 (2 nbar, (d)). Concerning XPS analysis, records of the V 2p core level are plotted in
7 Figure 2(e)-(h) for thin films deposited at different substrate temperatures and oxygen partial
8 pressures. For the highest $p(O_2)$ (400 nbar) and a deposition temperature of 400 °C (Figure 2e
9 green curve), vanadium V 2p core level spectra reveal a peak with a symmetric shape
10 associated to a single valence of V 5+ for V 2p_{1/2} as well as V 2p_{3/2}. For the same pressure
11 value and room temperature deposition (Figure 2e blue curve), a slight shift is recorded and
12 significant for a major valence of V 5+ with a minor component of V 4+ at lower binding
13 energy. Thin films sputtered at room temperature for three values of $p(O_2)$ (100 nbar, 10 nbar
14 and 6 nbar, Figure 2f) display very similar spectra with broad maxima located at a binding
15 energy associated to V 4+, meaning that components associated to V 5+ and V 3+ might also
16 have a contribution. In addition, the spectrum of a V_2O_3 thin film of sputtered at 600 °C and a
17 $p(O_2)$ of 10 nbar is given (red curve in Figure 2f). One can observe a shift of the broad
18 maximum of V 2p_{1/2} to a slightly lower binding energy associated with a shoulder located at
19 a binding energy of V 2+ (which is not recorded for thin films deposited at room temperature,
20 see blue curves). In the case of the thin film sputtered at 2 nbar $p(O_2)$ either at room
21 temperature or 400 °C (Figure 2g), one can observe a greater shoulder (~513 eV) of the
22 V 2p_{1/2} peak compared to crystalline V_2O_3 (Figure 2f red curve). Lastly, Figure 1h shows the
23

1 V 2p core level spectrum of a thin film sputtered at 0 nbar $p(\text{O}_2)$ (with an asymmetric peak
2 shape) as a reference for the V 2p binding energy of metallic vanadium.

3

4 **3.3 Temperature Profile of Vanadium Oxides Sputtered at 10 nbar $p(\text{O}_2)$**

5 The last presented sample series 4 has been deposited with an oxygen partial pressure of
6 10 nbar and a sputter power of 50 W for increasing substrate temperature between 50 °C and
7 600 °C. Deposition rates, detected phases as well as analysis of vanadium valence are given in
8 **Table 4**. Phase analysis was performed for an additional series 5 (with a sputtering power of
9 100 W, not shown) where XRD-analysis only exhibited diffraction peaks of corundum V_2O_3
10 (except for a deposition temperature of 400 °C where a mixture of bixbyite V_2O_3 was
11 obtained). In **Figure 3a**, the XRD patterns at grazing incidence angle are plotted versus
12 deposition temperature between 30 °C and 600 °C (with increasing value starting from the
13 bottom). As displayed in the bottom part of Figure 3a, the recorded pattern for samples
14 obtained in the 30 °C to 250 °C range only revealed diffraction peaks related to lattice planes
15 of cubic platinum [40] (resembling the bottom electrode) and can thus be characterized as X-
16 ray amorphous. As published previously [33], XPS-analysis of a thin film deposited at room
17 temperature revealed a mixture of several vanadium valences ranging from +3 and +5
18 (compare Figure 2f). For a deposition temperature of 300 °C, diffraction peaks associated to
19 the crystallization of corundum V_2O_3 can be identified at $\Theta = 24,5^\circ$, $33,2^\circ$ and $54,3^\circ$ which
20 correspond to $\{012\}/\{104\}/\{116\}$ - lattice planes. According to the JPCDS file of corundum
21 V_2O_3 , these diffraction peaks possess the highest relative intensities (66 %, 100 %, 86 %) of the
22 corundum-type V_2O_3 diffraction pattern [38]. Between 400 °C and 550 °C, several additional
23 diffraction peaks are recorded that predominantly belong to corundum-type V_2O_3 (Figure 3a
24 black squares). Yet, some remaining diffraction peaks not belonging to corundum-type V_2O_3

1 occur as well (Figure 3a marked by arrows). The diffraction peaks have been identified to
2 belong to a bixbyite-type V_2O_3 [41] phase and were reproducibly observed in multiple samples.
3 Figure 3b compares the crystal structures of bixbyite- and corundum-type V_2O_3 are illustrated
4 where grey spheres represent vanadium atoms and red spheres oxygen atoms. In addition,
5 Figure 3c shows a distinct X-ray diffraction pattern of a thin film (sputtered at 450 °C) with the
6 two coexisting V_2O_3 phases (where red and black vertical lines identify diffraction peaks
7 associated to bixbyite and corundum V_2O_3 phases, respectively). Based on XRD-analysis,
8 volume fractions of the two polymorphs were extracted by fitting diffraction profiles with
9 PowderCell (Figure 3d). As plotted, it appears that the higher content of bixbyite V_2O_3 phase
10 potentially reaches a maximum for a deposition temperature of 400 °C in our experimental
11 conditions and subsequently decreases for higher deposition temperatures. Interestingly, the
12 margin of volume fraction is the largest at this temperature and decreases with higher
13 deposition temperatures. For a deposition temperature of 600 °C, no bixbyite V_2O_3 phase has
14 been detected anymore. In contrast, for samples obtained at a sputtering power of 100 W in
15 the same oxygen partial pressure range (series 5), no bixbyite phase could be detected for the
16 same oxygen partial pressure except for a deposition temperature of 400 °C (see later in
17 Figure 6b). In the studied experimental range, the ratio between corundum and bixbyite phase
18 could vary considerably depending on deposition temperature, sputtering power and sample
19 batch. Major morphological changes were determined with respect to deposition
20 temperature by SEM imaging and are gathered in **Figure 4a-e**. Deposition at room
21 temperature (Figure 4c) resulted in an amorphous columnar structure (i.e. the classical
22 expected morphology of sputtered thin films) with a relatively broad distribution of the lateral
23 grain size of 40 ± 20 nm. For a substrate temperature of 400 °C (Figure 4b), the thin film
24 possesses a similar columnar grain growth mode even when crystallized in pure corundum

1 V_2O_3 (verified by XRD:GI). At a higher substrate temperature of 600 °C (Figure 4a), a change in
2 growth mode to globular grains with larger grain size (58 ± 20 nm) is observable and the
3 crystalline quality as well as the corundum V_2O_3 phase content reach a maximum in the
4 investigated range. At an intermediate substrate temperature of 300 °C (Figure 4d) where XRD
5 analysis reveal emerging diffraction peaks in a mainly amorphous structure, grains with a
6 length of ~ 100 nm and a sharp surface structure start to grow on the surface of the amorphous
7 bulk thin film. Figure 4e illustrates the nanostructure of the surface of the thin film with most
8 prominent bixbyite content of 78 ± 5 vol. % (compare with the thin film of pure corundum
9 phase in Figure 4b). As shown, a mainly inhomogeneous morphology is formed with large
10 grains (~ 50 nm diameter) which consist of several smaller grains (~ 10 nm diameter). A
11 schematic evolution of phase coexistence in deposited vanadium oxide thin films is presented
12 in Figure 4f through light microscopy images (with respect to temperature at the bottom of
13 the graph) showing two distinct regions. Up to a deposition temperature of 400 °C, a
14 continuous change in contrast is observed that correlates with the increase in density
15 (Figure 4g squares). Using deposition temperatures above 400 °C (at the beginning of bulk
16 crystallization), samples display the common black color of bulk V_2O_3 [42]. The evolution of
17 thin film parameters (density ρ , deposition rate dd/dt , root mean square roughness R_{ms} and
18 mean lateral grain size d_{GS}) is plotted in Figure 4g as function of deposition temperature. The
19 colored area is a visual guideline for the distribution of grain sizes d_{GS} . As fitted by XRR
20 measurements, the density ρ (Figure 4g dots) increases continuously from 3.5 to 4.5 g/cm³
21 with increasing deposition temperature. A stable maximum (4.5 g/cm³) is reached at 500 °C.
22 Amongst amorphous films, roughness (star symbols) decreases continuously up to 150 °C. For
23 amorphous films, the highest root mean square roughness R_{ms} (evaluated by AFM imaging)
24 was found for films deposited at room temperature ($R_{ms} = 2.4$ nm) whereas for (partially)

1 crystalline films from 200 °C upwards, roughness increases continuously from $R_{ms} = 1.9$ nm to
2 3.5 nm (in analogy to observed recrystallization at 600 °C, Figure 4a). At a deposition
3 temperature of 450 °C, a huge drop of average grain size d_{GS} (pentagon symbols) and an
4 increase in deposition rate are observed; meanwhile, a large fraction of bixbyite V_2O_3 equal to
5 36 vol. % occurs. In the temperature range of bulk crystallization (400 °C up to 550 °C), grain
6 size barely increases up to 45 nm. Finally at 600 °C, as the pure corundum V_2O_3 is obtained,
7 the largest observed mean grain size > 60 nm is reached.

8 **3.4 Morphology and Low Temperature Electrical Measurements of V_2O_3**

9 In **Figure 5**, SEM images in top view and cross section (a) and low temperature electrical
10 transport properties (b) are reported for thin films deposited at 100 W and a $p(O_2)$ of 10 nbar
11 for three deposition temperatures (30 °C / 400 °C / 600 °C) and for a sputtering power of 50 W
12 for the case of 600 °C.

13 For the lowest deposition temperature without heating (30 °C and $P = 100$ W), amorphous VO_x
14 exhibits a fine-grained microstructure with a random grain orientation as shown in cross-
15 section (Figure 5a(1)). The morphology is slightly different from the one observed for half the
16 sputter power of 50 W (Figure 4c) where columnar growth was highlighted. By increasing
17 deposition temperature to 400 °C ($P = 100$ W), numerous crystallite edges emerge on the
18 surface of a thin film (Figure 5a(2)) in agreement with crystallized V_2O_3 verified by XRD-
19 analysis (not shown). In contrast to the thin film deposited at the lower power of 50 W
20 (Figure 4a), the density of crystallite edges on the surface increases considerably. At a
21 deposition temperature of 600 °C, grain size increases to a maximum for both used powers of
22 100 W (Figure 5a(3)) and 50 W (Figure 5a(4)). In this case, no significant change of morphology
23 is visible between the two deposition power values. To get further insights, the electrical
24 transport characteristics of the same films have been acquired (Figure 5b). A purely insulating

1 behaviour has been evidenced for the vanadium oxide thin film sputtered at room
2 temperature at low oxygen partial pressure (Figure 5b(1)). For V_2O_3 thin films sputtered at
3 400 °C (Figure 5b(2) green curve), no transition can be detected. Only a slight increase in
4 resistance is recorded below 50 K. For the thin film with maximum bixbyite V_2O_3 content of
5 78 vol. % (Figure 5b(2) second green curve), the same characteristics are obtained. In contrast,
6 V_2O_3 thin films sputtered at 600 °C show an insulator to metal transition (IMT) with a
7 sputtering power of 100 W (Figure 5b(3)) and an insulator to semiconductor transition (IST)
8 with a sputtering power of 50 W (Figure 5b(4)). In the inset of Figure 5b, the diffraction peak
9 of the (220) lattice plane of platinum is depicted for two different deposition temperatures at
10 400 °C (green) and 600 °C (red). In both cases, fringes occur whereas the amplitude of fringes
11 increases considerably for a substrate temperature of 600 °C.

12

13 **4. Discussion**

14 In the following sections, physical properties of vanadium oxide thin films are discussed with
15 respect to variation of process parameters (namely oxygen partial pressure, deposition
16 temperature and sputtering power).

17

18 **4.1 Deposition Rate and Phase as Function of Sputtering Parameters**

19 In this section, chemical composition as function of $p(O_2)$ will be compared to their
20 corresponding deposition rates (Figure 1). Therefore, **Figure 6a** summarizes the evolution of
21 the average O/V ratios as function of oxygen partial pressure for the investigated deposition
22 conditions as determined by XRD and XPS analysis (Tables 1-4 and Figures 2-3). The observed
23 trend of deposition rate for amorphous and crystalline thin films with respect to $p(O_2)$
24 (Figure 1 blue dashed curve) has been reported previously for vanadium oxide thin films

1 deposited by pulsed DC magnetron sputtering [43] and RF magnetron sputtering [44][45]. In
2 regime (1) at high oxygen partial pressure above 200 nbar, it can be assumed that the entire
3 target and chamber walls are covered with oxide that prevents a significant change in
4 deposition rate. Concomitantly, only fully oxidized thin films (with chemical composition of
5 V_2O_5) were deposited at room temperature or a substrate temperature of 400 °C. In the so
6 called target oxidation regime around $p(O_2) = 100$ nbar (critical flow regime (2)), the
7 deposition rate increases drastically by roughly one order of magnitude which may be linked
8 to a strong decrease of target coverage with vanadium oxides of high O:V ratio close to 2.5. In
9 addition, amorphous samples show a transition from almost fully oxidized VO_x with $x \sim 2.4$ to
10 an average valence of +4 with $x = 2$. Crystalline thin films obtained at equivalent $p(O_2)$ exhibit
11 a similar change of oxidation state towards lower oxidation degree below VO_2 . With further
12 decrease of the oxygen partial pressure, a deposition rate plateau is reached (~ 8.5 nm/min)
13 associated to the intermediate flow regime (3) between a pressure range of 100 nbar and
14 10 nbar. In such conditions, only minor target oxidation occurs and is in good agreement with
15 the high value of deposition rate (~ 7 nm/min). In the same range, amorphous $VO_{x=2}$ with a
16 major valence of +4 (but also a mixture of valence +3 and +5 as shown in XPS analysis by the
17 broad V 2p peak width [33]) is the only phase present (Figure 2f). In the lowest range of $p(O_2)$
18 (10 to 1 nbar, regime (4)), the deposition rate can be lowered by the lack of oxygen necessary
19 to react with vanadium to form oxide products. The deposition rate of crystallized phases
20 changes more frequently with a variation of ~ 2 nm/min which is likely to be related to the
21 competition and coexistence of generated crystalline phases (also compare the sudden
22 increase in deposition rate with formation of bixbyite V_2O_3 at 450 °C, Figure 4). The largest
23 deposition rate (8.8 nm/min) was reached for thin films deposited at 400 °C with a sputtering
24 power of 100 W and an oxygen partial pressure of 70 nbar (regime (3)). Interestingly, this

1 deposition rate matches the intermediate plateau observed for amorphous thin films which
2 spans a broad range of 90 nbar $p(\text{O}_2)$. In the last regime below 10 nbar (regime (4)), film
3 growth takes place in an environment with very low oxygen flow and thus leads to a gradual
4 decrease of the deposition rate. In this region, crystalline phases with the lowest O:V ratio
5 such as V_2O_3 , VO or even pure V are deposited. The lowest oxidation state of vanadium (except
6 for a $p(\text{O}_2)$ of 0 nbar) was observed for 1 - 2 nbar $p(\text{O}_2)$ (Figure 2g / Table 1) with a similar
7 mixture of +2 and +3 valence for both deposition temperatures. In both cases, the base
8 pressure of the chamber (≈ 1 nbar) may already lead to post-process oxidation at the surface
9 of the thin film before the thin film is capped with gold. This process could explain a
10 termination with a major V_2O_3 spectrum even for crystalline thin films that show only single-
11 phased VO in X-ray analysis (Figure 2d&g). Previously published works align with the very
12 difficult control of pure amorphous vanadium 3+ within the investigated parameter range [25].
13 Thus, even though the trends in deposition rate variation of amorphous and crystalline films
14 are comparable, the stoichiometry of amorphous thin films in the intermediate flow regime
15 (3) might also be masked by a surface passivation with the more stable +4 valence. The same
16 trend can even be observed for the amorphous V_2O_5 thin film compared to the crystalline V_2O_5
17 thin film (Figure 2e) where only a small fraction of V 4+ valence is detected in the amorphous
18 thin film. A similar passivation effect was also observed by Bergerud et al. for (metastable)
19 crystalline bixbyite V_2O_3 when annealed at 120 °C for several minutes in ambient atmosphere,
20 i.e. containing oxygen [46]. The stoichiometry variation of (stable) crystalline phases versus
21 $p(\text{O}_2)$ is in agreement with a logarithmic dependence with respect to oxygen partial pressure.
22 In the stoichiometry regime of the desired V_2O_3 phase (e.g. between 3 and 20 nbar $p(\text{O}_2)$ at
23 400 °C in Figure 6a), a phase mixture between corundum and bixbyite V_2O_3 is predominantly
24 obtained (Figure 6b). The metastable bixbyite-type V_2O_3 phase has been synthesized by wet-

1 chemical processing [47] which was discovered ~~for the first time~~ only in the last decade. In
2 contrast to the well-known paramagnetic metallic corundum-type V_2O_3 phase, the
3 antiferromagnetic [48] semiconducting bixbyite-type V_2O_3 phase indeed exhibits the ability to
4 accommodate oxygen excess on interstitial sites [49]. Consequently, bixbyite-type V_2O_3 was
5 also proposed for oxygen storage systems [46]. So far, ~~to the best of our knowledge,~~ no other
6 method has been reported in literature for bixbyite V_2O_3 (and therefore no physical deposition
7 method for thin films). In the present study, the content of both polymorphs varied with all
8 investigated parameters, namely substrate temperature, power and oxygen partial pressure.
9 One could speculate that the reason for the huge variation of bixbyite content at 400 °C can
10 be attributed to its meta-stability. Indeed, this polymorph of V_2O_3 is only 0.07 eV less stable
11 per formula unit than the corundum phase and can thus be considered as dynamically stable
12 [50]. A further observation supports this hypothesis: bixbyite V_2O_3 -based thin films of this
13 study have been stored in nitrogen atmosphere with ~ 1 ppm O_2 over four years without
14 significant degeneracy of the bixbyite phase content. At a deposition temperature of 600 °C,
15 the bixbyite V_2O_3 content vanishes which is in agreement with published results on bixbyite
16 V_2O_3 nanoparticles synthesized by wet-chemical means [41]. These particles started to
17 transform to corundum V_2O_3 over hours/days in ambient atmosphere at room temperature
18 and over minutes in annealing conditions of up to 700 °C. For sputtered thin films, it is well
19 known that a significant decrease of deposition-induced defects (created under bombardment
20 with ionic species from the sputter gun) requires a certain mobility of atomic and ionic species
21 provided by increasing temperature or increasing the momentum transfer. Thus, with the help
22 of thermal activation and volume diffusion, the metastable phase can transform to the stable
23 corundum phase during grain growth. In the case of reactive sputtering, we show that not only
24 the increase deposition temperature but also lowering of the oxygen partial pressure and a

1 higher power lead to vanadium oxide thin films with a vanishing content of bixbyite V_2O_3 .
2 These results are interpreted by an increased reaction rate of vanadium with oxygen thanks
3 to increasing sputtering power or reducing oxygen partial pressure that both favor formation
4 of the stable corundum V_2O_3 phase over an oxygen-oversaturated bixbyite phase.

5

6 **4.2 Influence of Deposition Parameters on Morphology and Phase Composition**

7 Considerable changes in morphology are observed with variations in sputtering parameters
8 such as total pressure and substrate temperature as described by the Thornton Model [51].
9 At room temperature, the low surface mobility of ad-atoms leads to the commonly observed
10 columnar oriented grain growth (Figure 3b at 30 °C). For substrate temperatures above
11 300 °C, surface mobility additionally induces growth of single crystallites of corundum V_2O_3 on
12 top of the thin film (Figure 4a at 300 °C). Starting from 400 °C, crystallization of the entire thin
13 film is most likely initiated by atom diffusion along the (high density of) inter-columnar grain
14 boundaries. A possible impact of the creation of both polymorph V_2O_3 phases on grain growth
15 is highlighted in Figure 4. At a deposition temperature of 450 °C, the increase in deposition
16 rate is going along with a considerable reduction in average grain size which can originate from
17 competing nucleation of both corundum and bixbyite V_2O_3 in the thin film bulk (Figure 3a at
18 450 °C). With increasing deposition temperature up to 600 °C (Figure 3a at 600 °C), interfacial
19 energy is further reduced with globular grain growth (Figure 3a&b at 600 °C) by
20 recrystallization. At the same time, the stability of bixbyite V_2O_3 might be further lowered by
21 recrystallization of corundum V_2O_3 into large globular grains. In the case of bixbyite nano-
22 crystallites synthesized by wet-chemical processing, a critical size of transformation has been
23 evidenced between 27 nm and 42 nm and was accompanied by particle coarsening [41]. This
24 range of particle size is in agreement with the crystallite sizes observed in our films with an

1 average grain size of 29 nm for the mixed-phase V_2O_3 obtained at 450 °C compared to pure
2 corundum V_2O_3 synthesized at 600 °C with an average grain size of 63 nm. Our data are in
3 favour of the hypothesis of Bergerud et al. that the surface energy of bixbyite V_2O_3 needs to
4 be considerably smaller than the one of corundum V_2O_3 [41]. The stability of bixbyite V_2O_3 on
5 the lower end of the nanoscale could therefore prove an important factor for scaling of V_2O_3 -
6 based electrical devices below 10 nm. Only with a deposition temperature of at least 600 °C,
7 pure phase corundum V_2O_3 has been formed in the present study (Figure 6). Thus, deposition
8 temperatures above 550 °C may still favour the corundum phase of V_2O_3 on the nanoscale
9 when proper recrystallization takes place. Lastly, the core level spectrum of the V_2O_3 thin film
10 (Figure 2f red spectrum) matches the determined profile which was determined for a V_2O_3
11 single crystal [34]. Main features of the complex V_2O_3 phase profile are a broad distribution of
12 the core level peaks due to various multiplet configurations in the photoemission final states
13 (that are related to the core hole-3d electrons interaction) as well as a binding energy very
14 close to VO_2 with a slight decrease of only 0.15 eV [34]. Disproportionation and/or surface
15 defects can further complicate the interpretation of the obtained profile (e.g. the feature at a
16 binding energy of ~ 512.8 eV close to V $2+$ which indicates a phase content of VO at the very
17 surface).

18 **4.3 Electrical Properties of V_2O_3 as Function of Sputter Parameters**

19 Clearly, deposition parameters are expected to have a strong impact on material properties
20 an here in particular on the metallicity and the IMT of corundum V_2O_3 . In our study, it appears
21 that the (simplest, energetically and technically most favourable) deposition method at room
22 temperature leads to a purely semiconducting amorphous vanadium oxide phase
23 (Figure 5b(1)) exhibiting a columnar grain structure. Furthermore, the amorphous phase
24 contains a major fraction of +4 valence as checked by the broad V 2p peak width recorded by

1 XPS analysis (Figure 2f). Theoretically, the origin of the high amount of +4 in a large oxygen
2 partial pressure range could either stem from post-oxidation at the thin film surface, at least
3 in the sensitivity range of XPS, i.e. several nm. Still, this post oxidation step (which could only
4 be induced by the remaining base pressure) may only happen within the few seconds between
5 the end of the deposition process and subsequent capping. However, since the oxygen partial
6 pressure (i.e. the total amount of supplied oxygen) remained constant throughout series 4,
7 surface oxidation is not expected to be relevant for the bulk of the thin film. For higher
8 temperatures near the bulk crystallization temperature (400 °C), a phase mixture of corundum
9 V_2O_3 with bixbyite V_2O_3 could be observed. Therefore, it suggests itself that the atomic near-
10 neighbour orientation within the bulk of amorphous VO_x is close to one of a mixture between
11 corundum and bixbyite phase. This would mean an association of edge- and corner-shared
12 octahedral coordination of vanadium with oxygen. Thus, excess oxygen ($O:V > 1.5$) would
13 already be incorporated within the film and could eventually lead to the a competing
14 nucleation between both phase clusters. To validate this hypothesis, X-ray absorption
15 spectroscopy (e.g. EXAFS) could be performed to quantify coordination relationships. In
16 literature, this issue has been addressed for the iso-structural material of crystalline bixbyite-
17 type In_2O_3 [52]. Amongst additional studies mentioned in this work, the coordination of
18 oxygen around indium in the amorphous In_2O_3 phase is often compared to its equivalent
19 crystalline bixbyite counterpart. For vanadium oxide thin films synthesized with oxygen partial
20 pressures as low as 2 nbar (Figure 6a), a considerable contribution of vanadium +2 valence
21 turned amorphous thin films metallic (as verified by current-voltage sweeps, not shown). In
22 our case, this only leaves a theoretical $p(O_2)$ window between 2 nbar and 6 nbar for the
23 synthesis of pure amorphous V_2O_3 without secondary phases. Yet, phase valence mixtures
24 seem to be the most stable state for V 3+ in amorphous phases. Still, from an application point

1 of view (compare introduction part), the absence of vanadium oxide thin films with pure
2 amorphous +3 valence did not present a central issue in Cr-doped devices due to a stabilization
3 effect of Cr 3+ valence on the vanadium valence [33][53]. At the minimum crystallization
4 temperature of 400 °C, thin films grew in columnar structure (Figure 5a(2)&6a(2)) for both
5 sputtering powers of 50 W and 100 W. In this case, phase mixtures and point defects appear
6 to affect electrical properties in a large extent (Figure 5b). Principally, bixbyite V_2O_3 can still
7 be present in a large fraction as grain sizes are below the predicted critical particle size of
8 transformation [41]. When a pure corundum V_2O_3 phase is obtained, metallic behaviour is
9 stabilized and the IMT is observed only at temperatures below 50 K (Figure 5b(2)). The drop
10 of transition temperature down to such low values can be indicative of a vanadium defect
11 concentration in the range of 0.8 % – 3 % as observed for single crystals of V_2O_3 [54].
12 Alternatively, oxygen defects could play a role as well in a non-equilibrium synthesis process
13 such as reactive sputtering. In addition, in-plane compressive strain might be expected if
14 substrate-induced lateral restrictions of the columnar growth mode are present. However,
15 this scenario is only applicable for a textured growth mode of V_2O_3 where the a -plane
16 predominantly grows parallel to the surface [55]. Nearly identical electrical transport
17 behaviour was found in the thin film with a high bixbyite V_2O_3 content of 78 vol. %. (Figure 5b
18 marked green curve). DFT calculations predict semiconducting properties for pure bixbyite
19 V_2O_3 with a direct band gap of 0.8 eV [50] and an optical band gap of 1.29 eV determined by
20 UV-vis spectroscopy [41]. In the present case, it appears that the expected semiconducting
21 properties of (non-pure) bixbyite V_2O_3 is circumvented by a current flow through crystallites
22 of metallic corundum-type V_2O_3 across the MIM-geometry. In contrast, sputtered thin films
23 are well crystallized in globular grains when heated at 600 °C (Figure 4b(3)&5b(3)(4)) and
24 exhibit a metal-to-insulator transition up to four orders of magnitude (Figure 5b red curves).

1 As displayed, the transition spreads over a broad temperature range up to 135 K with a lower
2 (average) transition temperature of 100 K (compared to 155 K in bulk [8]) which either
3 indicates a strong defect gradient or stress gradient in the thin film. Both effects are likely to
4 be present at the same time. By entering the cooling period after the non-equilibrium
5 sputtering process of V_2O_3 , thermodynamics favour higher oxidized species such as VO_2 at a
6 base pressure of 10^{-7} mbar [56]. Moreover, thin film growth is likely to be influenced by
7 substrate-induced disorder through restricted columnar growth conditions on platinum [55].
8 For the two different deposition powers at 600 °C, slightly different growth conditions (with a
9 less dense microstructure of the thin film deposited at a sputtering power of 50 W) could
10 impose a tensile stress field (Figure 5b(4)) that could inhibit metallicity at room temperature
11 [55]. To get better insights on such effects in pure-phase corundum V_2O_3 , a more detailed
12 analysis of electronic transport properties with respect to lattice parameters and atomic
13 distribution has been conducted and will be published later on.

14

15 **4. Conclusion**

This work presents an extensive study of growth conditions and physical properties of vanadium oxide thin films by low temperature reactive sputtering (between 30 °C and 600 °C) with a focus on vanadium 3+ oxides. We highlight that morphology and stoichiometry can be directly controlled by experimental sputtering parameters such as oxygen partial pressure, substrate temperature and power supply. At the same time, electrical properties and phase composition are greatly affected. V_2O_3 thin films crystallized from 400 °C upwards. For substrate temperatures between 400 °C and 550 °C and a low power density of ~ 10 W/cm², a considerable fraction of a bixbyite V_2O_3 phase was detected with various content values. On the one hand, low sputtering power, high oxygen partial pressures (in the phase-pure regime

of V_2O_3) at a deposition temperature of 400 °C and low crystallization temperatures (400 °C) led to an increase of the bixbyite volume fraction up to 78 ± 5 vol. %. On the other hand, pure polycrystalline corundum V_2O_3 thin films were only obtained for a substrate temperature of 600 °C. Such polycrystalline thin films revealed a metal-to-insulator transition between 50 K and 150 K with a resistance ratio of four orders of magnitude and, depending on sputter power, diverging semiconducting or metallic properties. In the same investigated parameter range, XPS indicates that only mixed valences between +3 valence and other species such as +4 or +2 are stable in amorphous films. The mixed valence conditions are regarded as precursor of the polymorphism where bixbyite V_2O_3 can store excess oxygen interstitially. Thus, our deposition method gives access to a large range of vanadium oxidized-based thin films suitable for different applications such as resistive switching or oxygen storage systems. The relatively broad hysteresis width of ~ 100 K (Figure 5b) may be further reduced by quenching techniques [57]. To conclude, direct reactive sputtering involving a strongly diluted oxygen gas mixture can provide a fast and versatile one-step deposition process for corundum V_2O_3 .

Acknowledgements

J. A. J. Rupp would like to thank M. Rose and G. C. Huang for the support in sample preparation and measurement, K. Skaja, C. Bäumer, D. Bick and C. Rosário for discussions of XPS as well as B. Hadam from Institut für Halbleitertechnik (IHT) for providing SEM-images. Electrical measurements at low temperatures were performed at the Institut des Matériaux (IMN) in Nantes. J. A. J. Rupp thanks D. Babic (IMN) for measurement support and greatly acknowledges the Deutsche Forschungsgemeinschaft DFG for funding this project in the Sonderforschungsbereich (SFB) 917.

Bibliography

- [1] H. A. Wriedt, *Bull. Alloy Phase Diagrams* **1989**, *10*, 271. DOI: [10.1007/BF02877512](https://doi.org/10.1007/BF02877512).
- [2] M. Brahlek, L. Zhang, J. Lapano, H.-T.- Zhang, R. Engel-Herbert, *MRS Commun.* **2017**, *7*, 27. DOI: [10.1557/mrc.2017.2](https://doi.org/10.1557/mrc.2017.2).
- [3] P. Liu, K. Zhu, Y. Gao, H. Luo, L. Lu, *Adv. Energy Mater.* **2017**, *7*, 1700547. DOI: [10.1002/aenm.201700547](https://doi.org/10.1002/aenm.201700547).
- [4] R. T. Rajendra Kumar, B. Karunagaran, D. Mangalaraj, S. K. Narayandass, P. Manoravi, M. Joseph, V. Gopal, R. K. Madaria, J. P. Singh, *Int. J. Infrared Milli.* **2003**, *24*, 327. DOI: [10.1023/A:1021930717588](https://doi.org/10.1023/A:1021930717588).
- [5] G. Beydaghyan, V. Basque, P. V. Ashrit, *Thin Solid Films* **2004**, *522*, 204. DOI: [10.1016/j.tsf.2012.07.107](https://doi.org/10.1016/j.tsf.2012.07.107).
- [6] S. Kumar, M.D. Pickett, J.P.Strachan, G. Gibson, Y. Nishi, R. S. Williams, *Adv. Mater.* **2013**, *25*, 6128. DOI: [10.1002/adma.20130246](https://doi.org/10.1002/adma.20130246).
- [7] Y. Zhou, X. Chen, C. Ko, Z. Yang, C. Mouli, S. Ramanathan, *IEEE el. dev. lett.* **2013**, *34*, 202. DOI: [10.1109/LED.2012.2229457](https://doi.org/10.1109/LED.2012.2229457).
- [8] D. B. McWhan, A. Menth, P. Remeika, *J. Phys. Colloq.* **1971**, *32*, C1-1079. DOI: [10.1103/PhysRevB.7.1920](https://doi.org/10.1103/PhysRevB.7.1920).
- [9] P. Stoliar, L. Cario, E. Janod, B. Corraze, C. Guillot-Deudon, S. Salmon-Bourmand, V. Guiot, J. Tranchant, M. Rozenberg, *Adv. Mat.* **2013**, *25*, 23. DOI: [10.1002/adma.20130113](https://doi.org/10.1002/adma.20130113).
- [10] J. S. Brockman, L. Gao, B. Hughes, C. T. Rettner, M. G. Samant, K. P. Roche, S. S. P. Parkin, *Nature Nanotech.* **2014**, *9*, 453-458. DOI: [10.1038/nnano.2014.71](https://doi.org/10.1038/nnano.2014.71).
- [11] P. Stoliar, J. Tranchant, B. Corraze, E. Janod, M.-P. Besland, F. Tesler, M. Rozenberg, L. Cario, *Adv. Funct. Mater.* **2017**, 1604740, 1-7. DOI: [10.1002/adfm.201604740](https://doi.org/10.1002/adfm.201604740).
- [12] M. Querré, J. Tranchant, E. Janod, S. Cordier, V. Bouquet, S. Députier, M. Guilloux-Viry, M.-P. Besland, B. Corraze and L. Cario, *Phys. B.* **2017**. DOI: [10.1016/j.physb.2017.10.060](https://doi.org/10.1016/j.physb.2017.10.060).
- [13] C. Adda, L. Cario, J. Tranchant, E. Janod, M.-P. Besland, M. Rozenberg, P. Stoliar, B. Corraze, *MRS comm.*, **2018**, *8*, 835. DOI: [10.1557/mrc.2018.90](https://doi.org/10.1557/mrc.2018.90).
- [14] C.V. Ramana, S. Utsunomiya, R.C. Ewing, U. Becker *Sol. Stat. Commun.* **2006**, *137*, 645–649. DOI: [10.1016/j.ssc.2006.01.026](https://doi.org/10.1016/j.ssc.2006.01.026).
- [15] M. Querré, E. Janod, L. Cario, J. Tranchant, B. Corraze, V. Bouquet, S. Deputier, S. Cordier, M. Guilloux-Viry, M.-P. Besland, *Thin Solid Films* **2015**, *617*, 56-62. DOI: [10.1016/j.tsf.2015.12.043](https://doi.org/10.1016/j.tsf.2015.12.043).
- [16] F.Y. Kong, M.Li, D.B.Li, Y.Xu, Y.X.Zhang, G.H.Li, *J. Crys. Growth* **2012**, *346*, 22–26. DOI: [10.1016/j.jcrysgro.2012.02.039](https://doi.org/10.1016/j.jcrysgro.2012.02.039).
- [17] L. Dillemans, R.R. Lieten, M. Menghini, T. Smets, J.W. Seo, J.-P. Locquet, *Thin Solid Films* **2012**, *520*, 4730–4733. DOI: [10.1016/j.tsf.2011.11.64](https://doi.org/10.1016/j.tsf.2011.11.64).

- [18] S.A. Chambers, *Surf. Sci. Rep.* **2000**, 39, 105. DOI: [10.1016/S0167-5729\(00\)00005-4](https://doi.org/10.1016/S0167-5729(00)00005-4).
- [19] A.J. Window, A. Hentz, D.C. Sheppard, G.S. Parkinson, D.P. Woodruff, W. Unterberger, T.C.Q. Noakes, P. Bailey, M.V. Ganduglia-Pirovano, J. Sauer, *Surf. Sci.* **2012** 606 1716–1727. DOI: [10.1016/j.susc.2012.07.015](https://doi.org/10.1016/j.susc.2012.07.015).
- [20] A.-C. Dupuis, M. Abu Haija, B. Richter, H. Kuhlenbeck, H.-J. Freund *Surf. Sci.* **2003**, 539, 99–112. DOI: [10.1016/S0039-6028\(03\)00752-0](https://doi.org/10.1016/S0039-6028(03)00752-0).
- [21] H. Schuler, U. S. Klimm, G. Weissmann, C. Renner, S. Horn, *Thin Solid Films*, **1997**, 299, 119–124. DOI: [10.1016/S0040-6090\(96\)09399-6](https://doi.org/10.1016/S0040-6090(96)09399-6).
- [22] K. D. Rogers, J. A. Coath, M. C. Lovell, *J. Appl. Phys.* **1991**, 70, 1412. DOI:
- [23] K. Okimura, Y. Suzuki, *Jap. J. Appl. Phys.* **2011**, 50, 065803. DOI: [10.1143/JJAP.50.065803](https://doi.org/10.1143/JJAP.50.065803).
- [24] J. Brockman, M. G. Samant, K. P. Roche, S. S. P. Parkin, *Appl. Phys. Lett.* **2012**, 101, 051606. DOI: [10.1063/1.4742160](https://doi.org/10.1063/1.4742160).
- [25] B. D. Gauntt, E. C. Dickey, M. W. Horn, *J. Mater. Res.* **2009**, 24, 1590. DOI: [10.1557/jmr.2009.0183](https://doi.org/10.1557/jmr.2009.0183).
- [26] I. Yamaguchi, T. Manabe, T. Kumagai, W. Kondo, S. Mizuta, *Thin Solid Films* **2000**, 366, 294. DOI: [10.1016/S0040-6090\(00\)00740-9](https://doi.org/10.1016/S0040-6090(00)00740-9).
- [27] H. Poelman, H. Tomaszewski, D. Poelman, L. Fiermans, R. De Gryse, M.-F. Reyniers, G. B. Marin, *Surf. Interface Anal.* **2002**, 34, 724–727. DOI: [10.1002/sia.1397](https://doi.org/10.1002/sia.1397).
- [28] J. Trastoy, Y. Kalcheim, J. del. Valle, I. Valmianski, I. K. Schuller, *J. Mater. Sci.* **2018**, 53, 9131. DOI: [10.1007/s10853-018-2214-7](https://doi.org/10.1007/s10853-018-2214-7).
- [29] E. B. Thorsteinsson, S. Shayestehaminzadeh, U. B. Arnalds, *Appl. Phys. Lett.* **2018**, 112, 161902. DOI: [10.1063/1.5023180](https://doi.org/10.1063/1.5023180).
- [30] I. Valmianski, J. B. Ramirez, C. Urban, X. Batlle, I. K. Schuller, *Phys. Rev. B.* **2017**, 95, 155132. DOI: [10.1103/PhysRevB.95.155132](https://doi.org/10.1103/PhysRevB.95.155132).
- [31] J. E. Medvedeva, D. B. Buchholz, R. P. H. Chang, *Adv. Electron. Mater.* **2017**, 3, 1700082. DOI: [10.1021/cm502689x](https://doi.org/10.1021/cm502689x).
- [32] J. A. J. Rupp, R. Waser, D. J. Wouters, *Proc. 8th IEEE International Memory Workshop (IMW)* **2016**, pp. 37-40. DOI: [10.1109/IMW.2016.7495293](https://doi.org/10.1109/IMW.2016.7495293).
- [33] J. A. J. Rupp, M. Querré, A. Kindsmüller, M-P. Besland, E. Janod, R. Dittmann, R. Waser, D. Wouters, *J. Appl. Phys.* **2018**, 123, 044502. DOI: [10.1063/1.5006145](https://doi.org/10.1063/1.5006145).
- [34] M. Demeter, M. Neumann, W. Reichelt, *Surf. Sci.* **2000** 454-456, 41-44. DOI: [10.1016/S0039-6028\(00\)00111-4](https://doi.org/10.1016/S0039-6028(00)00111-4).
- [35] G. Silversmit, D. Depla, H. Poelman, G. B. Marin, R. De Gryse, *J. Electron. Spectrosc. Relat. Phenom.* **2004**, 135, 167. DOI: [10.1016/j.elspec.2004.03.004](https://doi.org/10.1016/j.elspec.2004.03.004).

- [36] Schulz, D., Larson, F., McCarthy, G., North Dakota State Univ., *ICDD Grant-in Aid* **1988**. ICDD 00-041-1426.
- [37] Andersson, G., *Acta Chem. Scand.*, **10**, 623, (1956), ICDD 01-072-0514.
- [38] *Natl. Bur. Stand. (U.S.) Monogr. 25*, **20**, 108, (1983), ICDD 00-034-0187.
- [39] Loehman, R.E., Rao, C.N.R., Honig, J.M., *J. Phys. Chem.*, **73**, 1781, (1969), ICDD 01-077-2173.
- [40] Barth, T., Lunde, G., *Z. Phys. Chem. Neue Folge. (Wiesbaden)* **1926**, 121, 78. ICDD 01-087-0640.
- [41] A. Bergerud, R. Buonsanti, J. L. Jordan-Sweet, D. J. Milliron, *Chem. Mater.* **2013**, 25, 3172. DOI: [10.1021/cm40153t](https://doi.org/10.1021/cm40153t).
- [42] M. D. Larrañaga, R. J. Lewis, R. A. Lewis, *Hawleys Condensed Chemical Dictionary* **2016**
- [43] J. A. Theil, E. Kusano, A. Rockett, *Thin Solid Films* **1997**, 298, 122. DOI: [10.1016/S0040-6090\(96\)09147-X](https://doi.org/10.1016/S0040-6090(96)09147-X).
- [44] P. Jin, S. Tanemura, *Jpn. J. Appl. Phys.* **1994**, 33, 1478. DOI: [10.1143/JJAP.33.1478](https://doi.org/10.1143/JJAP.33.1478).
- [45] H. Miyazaki, H. Sakamura, M. Kamei, I. Yasui, *Sol. Stat. Ion.* **1999**, 122, 223. DOI: [10.1016/S0167-2738\(99\)00022-3](https://doi.org/10.1016/S0167-2738(99)00022-3).
- [46] A. Bergerud, S. M. Selbach, D. J. Milliron, *ACS Nano* **2016**, 10, 6147. DOI: [10.1021/acsnano.6b02093](https://doi.org/10.1021/acsnano.6b02093).
- [47] D. Weber, A. Stork, S. Nakhal, C. Wessel, C. Reimann, W. Hermes, A. Müller, T. Ressler, R. Pöttgen, T. Bredow, R. Dronskowski, M. Lerch, *Inorg. Chem.* **2011**, 50, 6762. DOI: [10.1021/ic200799n](https://doi.org/10.1021/ic200799n)
- [48] D. Weber, C. Schwickert, A. Senyshyn M. Lerch, R. Pöttgen, *J. Mater. Res.* **2017**, 32,2397. DOI: [10.1557/jmr.2017.144](https://doi.org/10.1557/jmr.2017.144).
- [49] C. Reimann, D. Weber, M. Lerch, T. Bredow, *J. Phys. Chem.* **2013**, 117, 20164. DOI: [10.1021/jp406622u](https://doi.org/10.1021/jp406622u).
- [50] C. Wessel, C. Reimann, A. Müller, D. Weber, M. Lerch, T. Ressler, T. Bredow, R. Dronskowski, *J. Comput. Chem.* **2012**, 26, 2012-7.
- [51] J. A. Thornton, *J. Vac. Sci. A* **1986**, 4, 3059. DOI: [10.1116/1.573628](https://doi.org/10.1116/1.573628).
- [52] D. Bruce Buchholz, Q. Ma, D. Alducin, A. Ponce, M. Jose-Yacamán, R. Khanal, J. E. Medvedeva, R. P. H. Chang, *Chem. Mater.* **2014**, 26, 5401. DOI: [10.1021/cm502689x](https://doi.org/10.1021/cm502689x).
- [53] J. P. Pouget, H. Launois, *J. Phys. Colloques* **1976**, 37, C4-49. DOI: [10.1051/jphyscol.1976408](https://doi.org/10.1051/jphyscol.1976408).

[54] Y. Ueda, K. Kosuge, S. Kachi, *J. Sol. Stat. Chem.* **1980**, 31, 171. DOI: [10.1016/0022-4596\(80\)90019-5](https://doi.org/10.1016/0022-4596(80)90019-5).

[55] J. A. J. Rupp et al., to be published.

[56] Thomas B. Reed, *Free Energy of Formation of Binary Compounds*, MIT Press, Cambridge, MA, 1971.

[57] J. Trastoy, Y. Kalcheim, J. del Valle, I. Valmianski, I. K. Schuller, *J. Mater. Sci.* **2018**, 53, 9131. DOI: [10.1007/s10853-018-2214-7](https://doi.org/10.1007/s10853-018-2214-7).

Table 1: Low temperature deposition series 1: $T = 30\text{ }^{\circ}\text{C}$, $P = 100\text{ W}$ with deposition rate dd/dt and vanadium valence (as determined by XPS) as function of oxygen partial pressure $p(\text{O}_2)$.

Numbers in brackets are secondary valence states with minor quantitative occurrence.

$p(\text{O}_2)$ [nbar]	600	400	200	100	75	50	25	10	8	6	4	2	1	0
dd/dt [nm/min]	0.5	0.5	0.7	3	8.3	8.3	8.6	8	7	6.4	6	5.2	5	4.8
V valence		+5 (+4)		+4 (+3) (+5)				+4 (+3) (+5)		+4 (+3) (+5)			+3 (+2)	+0

Table 2: High temperature deposition series 2: $T = 400\text{ }^{\circ}\text{C}$, $P = 100\text{ W}$ with deposition rate dd/dt , detected phase and vanadium valence (as determined by XRD/ XPS, respectively) as function of oxygen partial pressure $p(\text{O}_2)$. For V_2O_3 , the fraction of bixbyite phase ($\text{V}_2\text{O}_3\text{ B}$) is indicated in volume percentage with an error of $\pm 5\text{ vol. \%}$. Ranges of vol. % are given for two samples. No ratio is available for 8-7.5 nbar due to low peak intensities (related to small grain sizes).

$p(\text{O}_2)$ [nbar]	1000	400	300	200	100	80	70	60	50
dd/dt [nm/min]	0.2	0.8	0.7	2	7.3	6.9	8.8	6.8	6.5
Phase(s) (XRD:GI)	V_2O_5	V_2O_5	V_2O_5	V_2O_5+ V_4O_7	V_4O_9 $+\text{V}_2\text{O}_5$	V_2O_5+ VO_2	VO_2	VO_2+ V_4O_9	VO_2+ V_4O_9
V Valence		+5					+4		
$p(\text{O}_2)$ [nbar]	40	12	11	10	9	8	7.5	7	6
dd/dt [nm/min]	7	7.3	7.6	7	7	6.5	6.2	6.4	6.6

Phase(s)	VO ₂ + V ₇ O ₁₃	V ₂ O ₃							
V ₂ O ₃ B [vol. %]	-	87	88	0-90	60-61	n.a.	n.a.	0	0
V Valence									

Table 3: High temperature deposition series 3: $T = 400\text{ }^{\circ}\text{C}$, $P = 50\text{ W}$ with deposition rate dd/dt , detected phase and vanadium valence (as determined by XRD/ XPS, respectively) as function of oxygen partial pressure $p(\text{O}_2)$. For V₂O₃, the fraction of bixbyite phase (V₂O₃ B) is indicated in volume percentage with an error of $\pm 5\text{ vol. \%}$.

$p(\text{O}_2)$ [nbar]	30	20	10	9	8	7	6
dd/dt [nm/min]	3.4	3.4	4.5	3.7	3.5	3.1	3.1
Phase(s) (XRD:GI)	V ₅ O ₉ + V ₂ O ₃	V ₂ O ₃ + V ₅ O ₉	V ₂ O ₃	V ₂ O ₃	V ₂ O ₃	V ₂ O ₃	V ₂ O ₃
V ₂ O ₃ B [vol. %]	-	-	78	80	n.a.	79	0
V Valence ($T=600\text{ }^{\circ}\text{C}$)			+3				
$p(\text{O}_2)$ [nbar]	5	4	3	2	1		
dd/dt [nm/min]	2.9	3.3	3.4	2.8	3.5		
Phase(s) (XRD:GI)	V ₂ O ₃	V ₂ O ₃ + +VO	V ₂ O ₃ + +VO	VO	V +VO		
V ₂ O ₃ B [vol. %]	n.a.	-	-	-	-		
V Valence				+2			

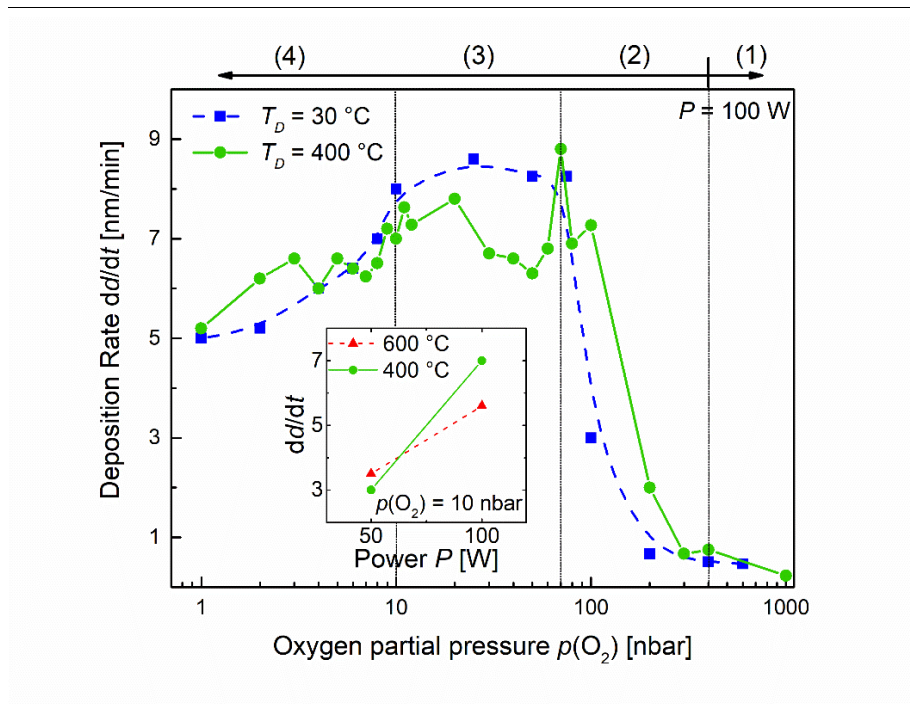


Figure 1: Deposition rate dd/dt as function of oxygen partial pressure $p(O_2)$ series of reactively sputtered VO_x , series 1: Films sputtered at room temperature $T_D = 30\text{ }^\circ\text{C}$ (blue squares with dashed line) and series 2: sputtered at elevated temperature $T_D = 400\text{ }^\circ\text{C}$ (green dots with solid line). Four different sputtering regimes are marked with (1)-(4). ***Inset:*** Deposition rate obtained with an oxygen partial pressure of 10 nbar for two deposition temperatures (400 °C and 600 °C in green and red, respectively) and two sputtering powers (50 W and 100 W).

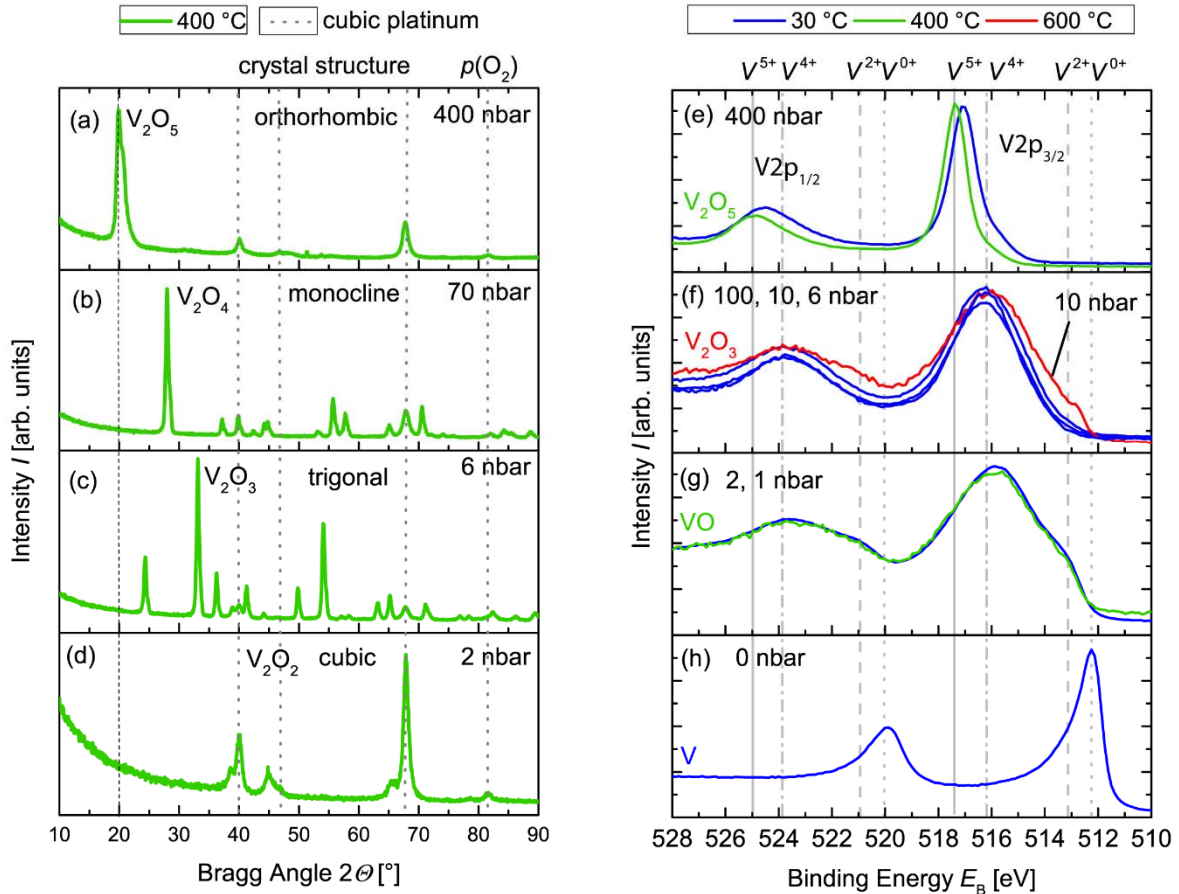


Figure 2: (a)-(d): X-ray diffraction patterns of pure phases with integer vanadium valence deposited on platinum (dotted lines) at 400 °C. Detected phases with respect to oxygen partial pressure: (a) V_2O_5 ^[36] at 400 nbar, (b) VO_2 ^[37] at 70 nbar, (c) V_2O_3 ^[38] at 6 nbar and (d) VO ^[39] at 2 nbar. Dashed vertical lines correspond to platinum planes^[40]. (e)-(h): Vanadium 2p core level spectra of thin films sputtered at room temperature (blue), 400 °C (green) and 600 °C (red) for different oxygen partial pressures: (e) 400 nbar, (f) 100 - 6 nbar, (g) 1-2 nbar and (h) 0 nbar. Spectra of crystalline thin films are marked with the stoichiometry which is expected by their crystallographic phase (that was determined by XRD). Phases with mixed valences between V +2 and V +4 present more complex core level spectra which are discussed in sections 4.1&4.2.

Table 4: Temperature series 4 with $P = 50$ W, $p(\text{O}_2) = 10$ nbar and deposition rate dd/dt , detected phase and vanadium valence (as determined by XRD/XPS, respectively) as function of oxygen partial pressure $p(\text{O}_2)$. For V_2O_3 , the fraction of bixbyite phase (V_2O_3 B) is indicated in volume percentage with an error margin of about ± 5 vol. %. Ranges are based on 2 samples per temperature between 400 and 550 °C.

T [°C]	50	100	150	200	250	300	350
dd/dt [nm/min]	4	3.9	3.9	3.9	3.7	3.8	3.6
Phase(s) (XRD:GI)	X-ray amorphous (distorted octahedral network)				(V_2O_3 , surf.)	(V_2O_3 , surf.)	(V_2O_3 , surf.)
V_2O_3 B [vol.%]					0	0	0
V Valence	+4						
T [°C]	400	450	500	550	600		
dd/dt [nm/min]	3.3	3.7	3.5	3.5	3.5		
Phase(s) (XRD:GI)	V_2O_3	V_2O_3	V_2O_3	V_2O_3	V_2O_3		
V_2O_3 B [vol.%]	0-78	18-36	4-15	0-11	0		
V Valence					+3		

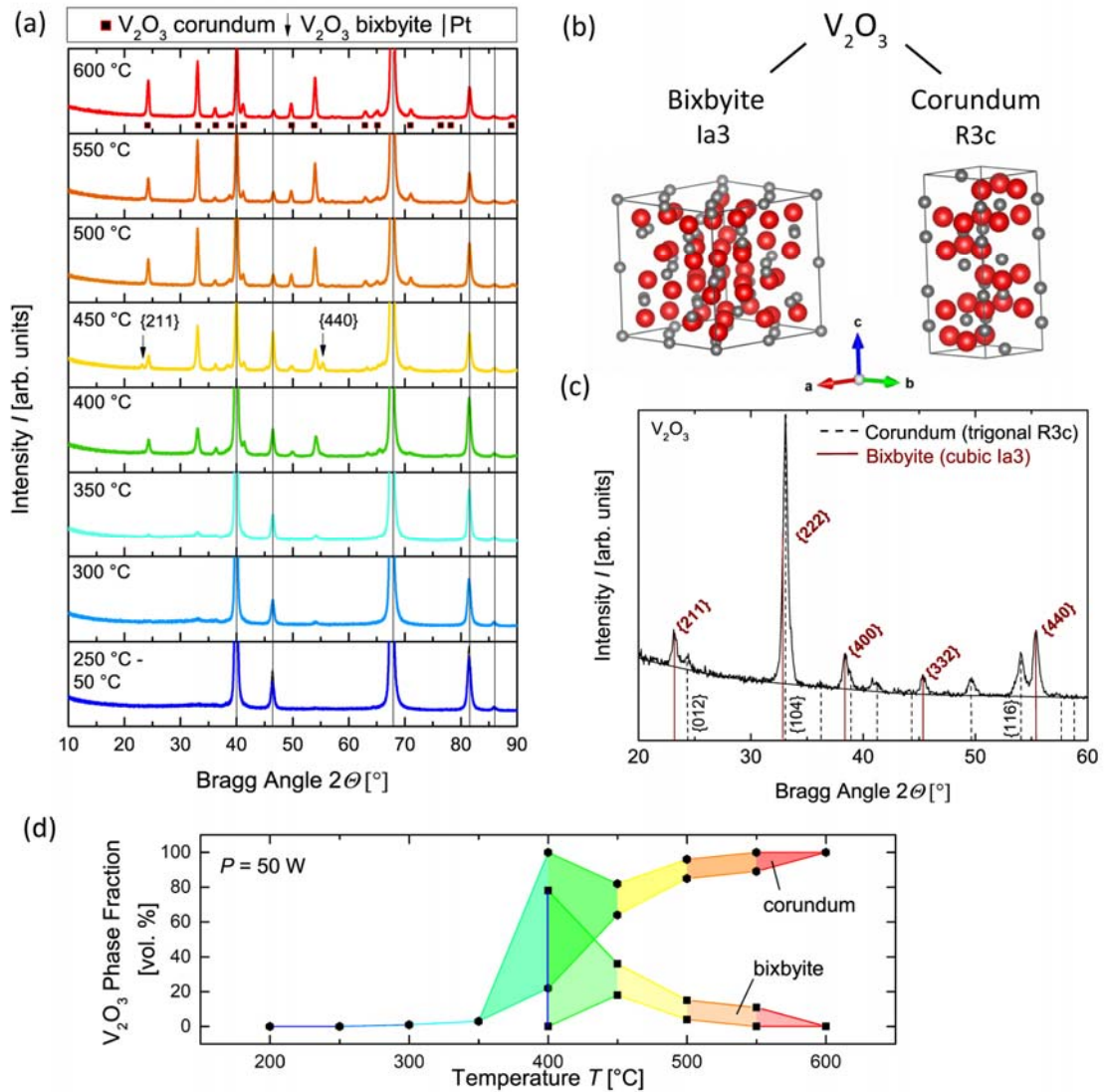


Figure 3: (a) XRD:GI measurement of 100 nm vanadium oxide thin films sputtered at 10 nbar oxygen partial pressure on a 30 nm thick platinum electrode with a sputtering power of 50 W. The substrate temperature is ranging from 30 °C up to 600 °C. Arrows indicate {211} and {440} lattice planes of bixbyite V_2O_3 at 23.1° and 55.5°, respectively^[41]. (b) Unit cells of V_2O_3 polymorphs bixbyite and corundum V_2O_3 . Small grey circles represent vanadium atoms and big red circles oxygen atoms. (c) Diffraction pattern of a thin film exhibiting a pronounced phase mixture. (d) Temperature dependent phase fraction of bixbyite and corundum-structured V_2O_3 (with each point representing a single sample).

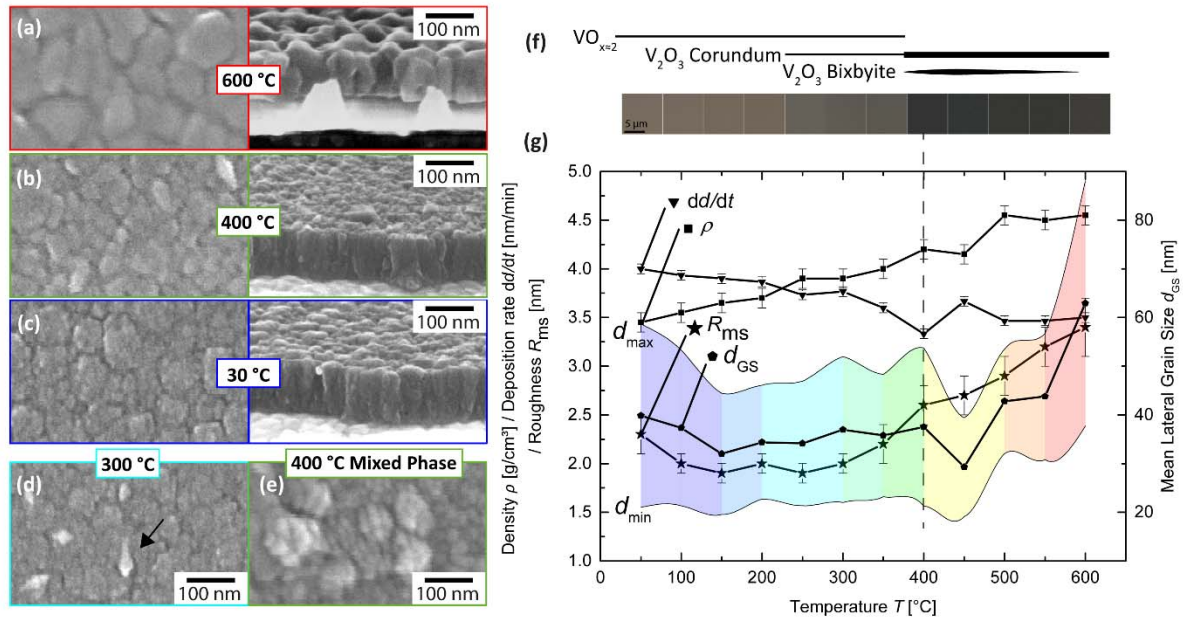


Figure 4: (a) SEM images: Top view (left) and cross section (right) of 100 nm thick vanadium oxide thin films deposited at 600 °C (a), 400 °C (b) and 30 °C (c) on 30 nm platinum with a sputtering power of 50 W, process pressure of 10 μbar and oxygen partial pressure of 10 nbar. An intermediate substrate temperature of 300 °C (d) reveals nucleation of corundum nanocrystallites on the surface (marked by an arrow). (e) Top-view of the nanostructure of V_2O_3 thin film with largest bixbyite volume fraction of 78 ± 5 vol. %. (f) Top: Qualitative volume fractions of phases marked by lines. Bottom: Light microscopy images of thin films under constant clean room yellow lightning. (g) Thin films properties, namely density ρ , deposition rate dd/dt , **root** mean square roughness R_{rms} and mean lateral grain size d_{GS} with respect to deposition temperature. The colored area marks the obtained grain size distribution.

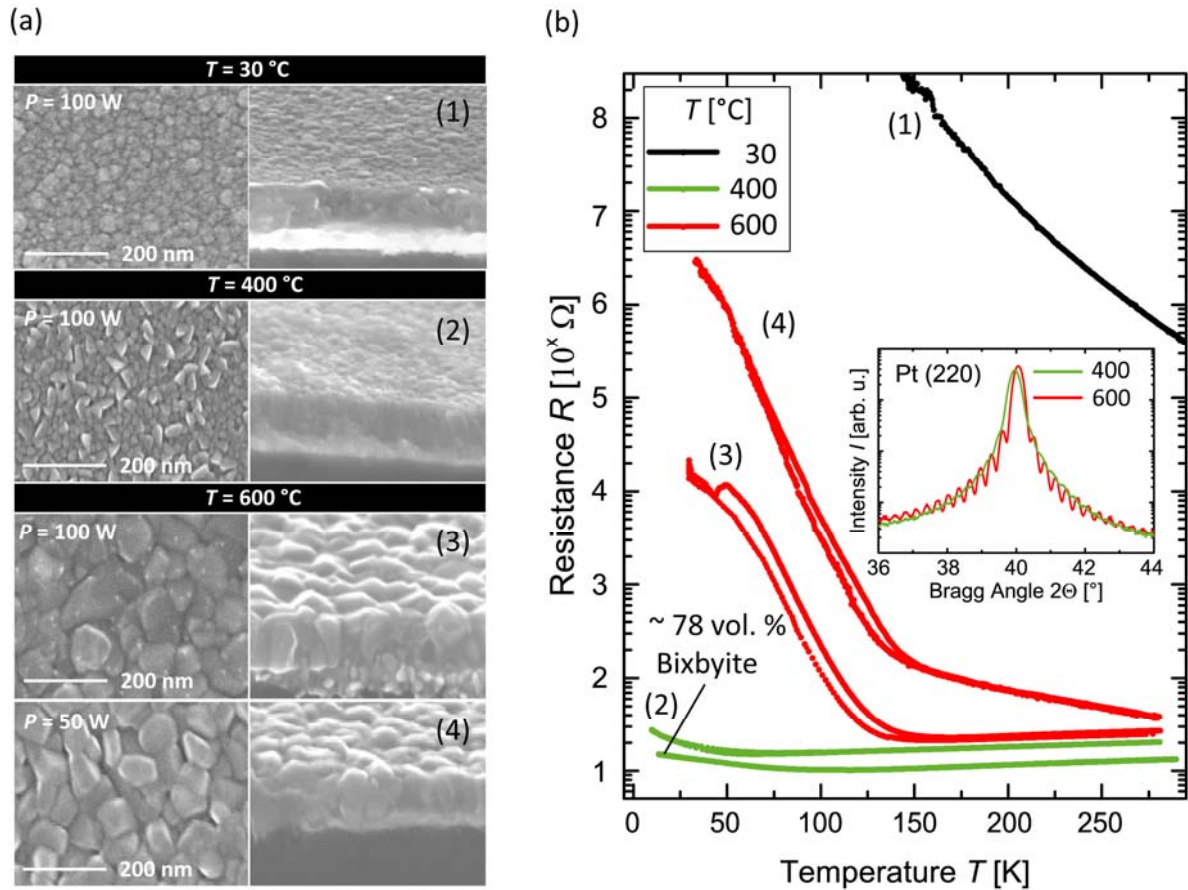


Figure 5: Morphological and electrical properties of amorphous VO_x and crystalline V_2O_3 thin films sputtered on platinum at different substrate temperatures and two sputtering powers. (a) SEM Top view (left) and cross section (right) of thin films obtained at $30\text{ }^{\circ}\text{C}$ with a power of 100 W (1), at $400\text{ }^{\circ}\text{C}$ with a power of 100 W (2) and deposited at $600\text{ }^{\circ}\text{C}$ with a power of 100 W (3) and 50 W (4). (b) Corresponding low temperature electronic transport properties marked by the same numbering. For a deposition temperature of $400\text{ }^{\circ}\text{C}$, two samples with pure corundum V_2O_3 and 78 vol. \% bixbyite V_2O_3 (compare Figure 4e) are compared. Inset: XRD:GI measurement of Pt {220} lattice plane diffraction peak with pronounced fringes.

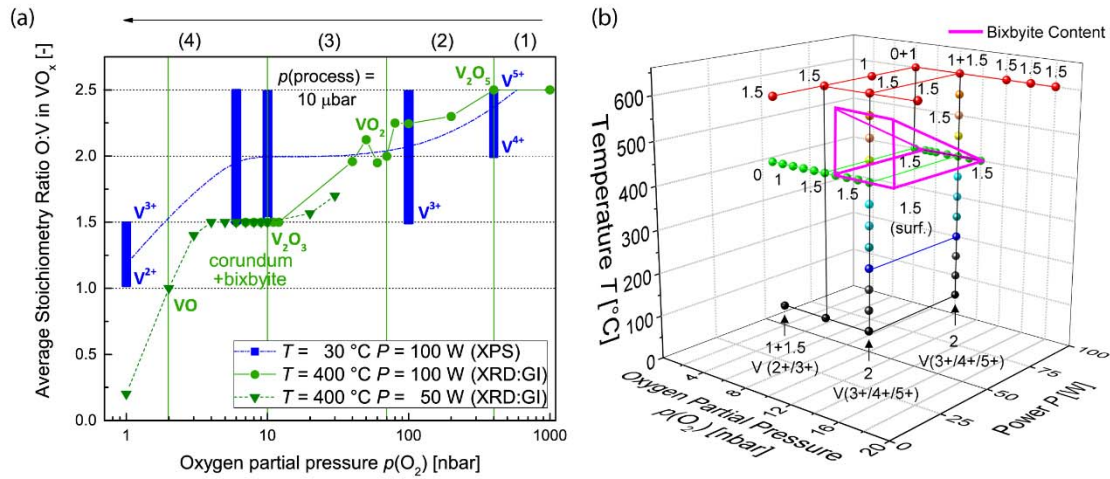


Figure 6: (a) Optical guidelines of average O:V ratios of deposited thin films in amorphous (blue line, 30°C) and crystalline (green, 400°C) form as function of oxygen partial pressure. Green dots mark averaged stoichiometries and blue bars the range of vanadium valences in amorphous films. The different ranges of deposition rates from Figure 1 are marked equivalently with (1) to (4). (b) 3D plot of oxygen:vanadium ratio as function of oxygen partial pressure, sputtering power and substrate temperature in the vicinity of V_2O_3 (O:V = 1.5) with detected bixbyite content (magenta region). For the determination of the stoichiometry matrix (marked by dots), some additional samples have been included which were analyzed by XRD:GI (not shown).